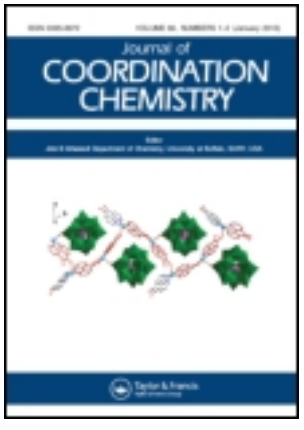

Journal of Coordination Chemistry
Publication details, including instructions for authors and subscription information:
http://www.tandfonline.com/loi/gcoo20

A 3-D Mn(II) complex containing N-isonicotinyl, N′,N′′-bis(hexamethylenyl) phosphoric triamide ligand: synthesis, structural characterization, and thermal studies

Khodayar Gholivand[a], Maryam Rajabi[a], Foroogh Molaei[a], Hamid Reza Mahzouni[a] & Sedigheh Farshadian[a]

[a] Faculty of Sciences, Department of Chemistry, Tarbiat Modares University, Tehran, Iran

Accepted author version posted online: 09 Nov 2013.Published online: 04 Dec 2013.

To cite this article: Khodayar Gholivand, Maryam Rajabi, Foroogh Molaei, Hamid Reza Mahzouni & Sedigheh Farshadian (2013) A 3-D Mn(II) complex containing N-isonicotinyl, N′,N′′-bis(hexamethylenyl) phosphoric triamide ligand: synthesis, structural characterization, and thermal studies, Journal of Coordination Chemistry, 66:23, 4199-4210, DOI: 10.1080/00958972.2013.863879

To link to this article: http://dx.doi.org/10.1080/00958972.2013.863879

Journal of Coordination Chemistry, 2013
Vol. 66, No. 23, 4199–4210, http://dx.doi.org/10.1080/00958972.2013.863879

A 3-D Mn(II) complex containing N-isonicotinyl, N′,N″-bis (hexamethylenyl) phosphoric triamide ligand: synthesis, structural characterization, and thermal studies

KHODAYAR GHOLIVAND*, MARYAM RAJABI, FOROOGH MOLAEI, HAMID REZA MAHZOUNI and SEDIGHEH FARSHADIAN

Faculty of Sciences, Department of Chemistry, Tarbiat Modares University, Tehran, Iran

(*Received 3 February 2013; accepted 29 October 2013*)

A new phosphoryl-containing ligand, N-isonicotinyl, N′,N″-bis(hexamethylenyl) phosphoric triamide (**1**), was synthesized and characterized using IR, ^{1}H, ^{13}C, and ^{31}P NMR and UV–vis spectroscopy. Reaction of **1** with $MnCl_2{\cdot}4H_2O$ led to the formation of Mn(II) complex with the formula $\{Mn[4\text{-}NC_5H_4C(O)NHP(O)(NC_6H_{12})_2]_2Cl_2\}_n$ (**2**). Crystal structures of **1** and **2** were determined by X-ray crystallography, which reveals that **2** is centrosymmetric with two phosphoryl oxygens, chloride and nitrogen in *trans* positions. Coordination of bridged bidentate **1** through oxygen of the phosphoryl and nitrogen of the pyridine afforded a 3-D network extended by coordinative bonds. Compound **2** and its nano-sized particles prepared by sonochemical method were characterized by IR spectroscopy, X-ray powder diffraction, and thermal analysis and exhibited paramagnetic behavior at room temperature. Crystalline mixture of $Mn_2P_2O_7$ and $Mn_2P_4O_{12}$ was identified as a thermolysis product of **2**.

Keywords: Mn(II) complex; Phosphoric triamide; Crystal structure; 3-D Network; Nano-sized particle

1. Introduction

Coordination chemistry of carbacylamidophosphates (CAPh), compounds containing –C(O)NHP(O)– with potential applications in pharmacological and agricultural industries [1–3], has significant growth. These ligands can bind to metal as *O*,*O*′–bidentate chelates in neutral [4, 5] and deprotonated form [6] or in a monodentate fashion via oxygen of the phosphoryl group [7–9]. Polymeric coordination compounds have been obtained by coordination of CAPh as η^2–bridged bidentate ligand [10] or by incorporating additional bridging ligands in the structure of CAPh [11].

Among 3d transition metals, there is an increased interest in manganese complexes due mainly to its importance in biochemistry and magnetism [12–16]. In coordination chemistry of CAPh, various complexes with s-, p-, d-, and f-metals have been structurally investigated [17–20]. However, there is only one reported Mn(II) complex with $(CCl_3C(O)NP(O)[NHC_3H_5]_2)$ [21], where coordination through oxygen of both phosphoryl and carbonyl resulted in a six-membered metallocycle. A limited number of Mn(II) complexes containing –(X)PNP(O)– group (X = S, O) [22–25] have also been reported. Generally, the structural

*Corresponding author. Email: gholi_kh@modares.ac.ir

differences of these compounds depend on the nature of the organic groups and chalcogens attached to phosphorus. Most of the foregoing complexes show discrete molecular structures, and polymeric ones are scarce.

In previous work, we reported synthesis of a series of CAPh ligands including isonicotinamide and nicotinamide groups, which possess pyridinic nitrogen as a new potential donor. Different coordination modes of these ligands were observed with Sn [26] and Er [27] showing molecular and polymeric structures, respectively. To find out more about the coordination diversity of pyridine containing CAPh, a new carbacylamidophosphate (**1**) was synthesized and characterized. The structures of **1** and its Mn(II) complex (**2**) were determined by X-ray crystallography. Since nanocoordination polymers exhibit properties distinct from their bulk counterparts [28], nano-sized particles of **2** were synthesized under ultrasonic irradiation. Use of CAPh for preparing inorganic nano-structured coordination polymers has not been investigated until now. Magnetic and thermal properties of bulk and nano-sized particles of **2** were studied and compared.

2. Experimental

2.1. *Materials and physical techniques*

All chemicals and solvents were of reagent grade and obtained commercially without purification. IR spectra were recorded on a Nicolet 510P spectrophotometer using KBr disks. ^{1}H, ^{13}C, and ^{31}P NMR spectra were recorded on a Bruker Avance DRX500 spectrometer. ^{1}H and ^{13}C chemical shifts were measured relative to internal TMS, and ^{31}P chemical shift relative to 85% H_3PO_4 as an external standard. UV–vis spectra were recorded on a Shimadzu UV-2100 spectrometer. Elemental analysis was carried out using a Heraeus CHN-O-RAPID apparatus. Melting points were obtained with an electrothermal instrument. X-ray powder diffraction (XRD) patterns were acquired using a Philips X′pert and STOE Theta-Theta diffractometer with monochromated Cu Kα radiation. The samples were characterized by a scanning electron microscope (SEM) S-4160 with gold coating and transmission electron microscope (TEM) Philips CM 30. A TECNO-GAZ S.P.A. Tecna 6, input: 50–60 Hz/138 W, was used for ultrasonic irradiation. Thermogravimetry (TG) and differential thermal analysis (DTA) were performed with a PL-STA 1640 system (5 °C/min heating rate under air). Magnetic measurements were carried out at room temperature using a vibrating sample magnetometer. X-ray data were collected on a Bruker SMART 1000 CCD [29, 30] for **1** and on a Bruker SMART APEX2 CCD area detector [31] for **2** with graphite-monochromated Mo Kα radiation (λ = 0.71073 Å). The structures were solved by direct methods and refined with full-matrix least-squares on F^2 by SHELXTL [32, 33]. All non-hydrogen atoms were refined anisotropically. The positions of hydrogens were obtained from the difference Fourier map. The crystal data and experimental details of the structure determinations for both compounds are listed in table 1.

2.2. *Synthesis of N-isonicotinyl, N′,N″-bis(hexamethylenyl) phosphoric triamide, 4-$NC_5H_4C(O)NHP(O)(NC_6H_{12})_2$ (1)*

N-isonicotinyl phosphoramidic dichloride, 4-$NC_5H_4C(O)NHP(O)Cl_2$, was prepared and purified according to the literature [34].

A solution of 4 mM hexamethyleneimine (0.40 mL) in 10 mL dry acetonitrile was added dropwise to a solution of 1 mM 4-$NC_5H_4C(O)NHP(O)Cl_2$ (0.24 g) in 20 mL acetonitrile at

Table 1. Crystallographic data for **1** and **2**.

Compound	**1**	**2**
Empirical formula	$C_{18}H_{29}N_4O_2P$	$C_{36}H_{58}Cl_2MnN_8O_4P_2$
Formula weight	364.42	854.68
Temperature (K)	120(2)	100(2)
Wavelength (Å)	0.71073	0.71073
Crystal system	Triclinic	Hexagonal
Space group	$P\bar{1}$	$R\bar{3}$
a (Å)	10.6110(11)	30.6676(7)
b (Å)	10.6433(12)	30.6676(7)
c (Å)	10.6495(11)	11.6356(5)
α (°)	63.615(2)	90
β (°)	76.574(3)	90
γ (°)	61.223(2)	120
V (Å^3)	944.11(17)	9477.2(5)
Z	2	9
Absorption coefficient (mm^{-1})	0.165	0.563
F(000)	392	4059
Crystal size (mm^3)	0.30 × 0.10 × 0.03	0.32 × 0.23 × 0.14
θ (°)	2.14–29.00	2.30–28.99
Index ranges	$-14 \le h \le 14$ $-14 \le k \le 14$ $-14 \le l \le 14$	$-41 \le h \le 41$ $-41 \le k \le 41$ $-15 \le l \le 15$
Reflections collected	10,499	32,992
Independent reflections	5003 [R(int) = 0.0317]	5510 [R(int) = 0.0521]
Completeness to theta (%)	99.5	98.4
Absorption correction	Semi-empirical from equivalents	Semi-empirical from equivalents
Refinement method	Full-matrix least-squares on F^2	Full-matrix least-squares on F^2
Data/restraints/parameters	5003/0/258	5510/5/300
Goodness-of-fit on F^2	1.002	1.050
Final R indices	R_1 = 0.0542, wR_2 = 0.1073	R_1 = 0.0386, wR_2 = 0.0957
R indices (all data)	R_1 = 0.0801, wR_2 = 0.1153	R_1 = 0.0591, wR_2 = 0.1046
Largest diff. peak and hole (e.Å^{-3})	0.388 and –0.369	0.429 and –0.355

0 °C. After 4 h of stirring, the solvent was evaporated and the residue washed with distilled water. Colorless needle crystals suitable for X-ray analysis were obtained in an NMR tube by crystallization from DMSO-d_6 solution. Yield: 88% (0.32 g). m.p. 155–157 °C. Anal. Calcd for $C_{18}H_{29}N_4O_2P$: C, 59.33; H, 8.02; N, 15.37. Found: C, 59.29; H, 7.95; N, 15.35%. ^{1}H NMR (500.13 MHz, DMSO-d_6): δ = 1.53–1.59 (m, $16H_{aliphatic}$), 3.05–3.17 (m, $8H_{aliphatic}$), 7.79 (d, $^3J_{HH}$ = 5.8 Hz, $2H_{pyridine}$), 8.71 (d, $^3J_{HH}$ = 5.8 Hz, $2H_{pyridine}$), 9.53 (s, 1H, NH_{amide}) ppm. ^{13}C NMR (125.76 MHz, DMSO-d_6): 26.23 (s), 29.68 (d, $^3J_{PC}$ = 3.7 Hz), 46.99 (d, $^2J_{PC}$ = 4.5 Hz), 121.65 (s), 141.04 (d, $^3J_{PC}$ = 8.0 Hz, C_{ipso}), 150.11(s), 166.82 (s, C=O) ppm. ^{31}P NMR (200.15 MHz, DMSO-d_6): 12.16 (m) ppm. IR (KBr, cm^{-1}): 3365 (br), 3064 (br), 2925 (s), 2856 (s), 1677 (s, C=O), 1598 (w), 1552 (w), 1500 (m), 1454 (vs), 1374 (m), 1341(m), 1278 (m), 1232 (m), 1193 (s, P=O), 1113 (m), 1059 (s), 1003 (m), 994 (m), 835 (m), 762 (w), 709 (m), 658 (w), 553 (w), 529 (w), 506 (w), 456 (w). UV–vis in methanol: λ_{max} = 263.5 nm.

2.3. *Synthesis of bis-[N-isonicotinyl, N',N''-bis(hexamethylenyl) phosphoric triamide] manganese(II) dichloride, {Mn[4-NC$_5$H$_4$C(O)NHP(O)(NC$_6$H$_{12}$)$_2$]$_2$Cl$_2$}$_n$ (2)*

0.5 mM $MnCl_2 \cdot 4H_2O$ (0.1 g) was added to a solution of 1 mM **1** (0.36 g) in 15 mL methanol and stirred for 4 h. X-ray quality crystals were isolated by slow evaporation of the solvent at room temperature. Yield: 50% (0.21 g). m.p. 204–206 °C. Anal. Calcd for $C_{36}H_{58}Cl_2MnN_8O_4P_2$: C, 50.59; H, 6.84; N, 13.11. Found: C, 50.68; H, 6.79; N, 13.17%.

IR (KBr, cm^{-1}): 3493 (br), 3065 (br), 2923 (s), 2861 (m), 1686 (s, C=O), 1610 (w), 1549 (w), 1458 (vs), 1377 (w), 1343 (w), 1276 (m), 1179 (s, P=O), 1118 (m), 1062 (s), 1006 (m), 942 (m), 861 (m), 824 (m), 754 (w), 712 (w), 552 (m), 483 (m), 428 (w). UV–vis in methanol: λ_{max} = 230 nm.

2.4. *Synthesis of $\{Mn[4\text{-}NC_5H_4C(O)NHP(O)(NC_6H_{12})_2]_2Cl_2\}_n$ (2) nano-sized particles by ultrasonic irradiation*

A solution of 0.5 mM $MnCl_2{\cdot}4H_2O$ in 10 mL 2-propanol was poured dropwise into a suspension of 1 mM **1** in hexane under ultrasonic irradiation (50–60 Hz/138 W) for 90 min. The obtained nano-sized product was filtered and air dried. m.p. 195–197 °C (Found: C, 50.74; H, 6.77; N, 13.19%), IR (KBr, cm^{-1}): 3429 (br), 3120 (br), 2925 (s), 2857 (m), 1683 (s), 1614 (w), 1557 (w), 1501 (m), 1455 (s), 1381 (m), 1271 (m), 1173 (s), 1114 (m), 1062 (s), 1006 (w), 942 (w), 835 (w), 706 (m), 530 (m), 488 (w), 428 (w).

Bulk powder and nano-sized particles of **2** were calcined at 600 °C in an electrical furnace under static air for 4 h. This process resulted in the formation of a mixture of $Mn_2P_2O_7$ and $Mn_2P_4O_{12}$. IR (KBr, cm^{-1}): 1641 (w), 1278 (m), 1090 (vs), 951 (s), 710 (w), 527 (m).

3. Results and discussion

3.1. *Spectroscopic study*

Synthesis of $4\text{-}NC_5H_4C(O)NHP(O)(NC_6H_{12})_2$ (**1**) was performed according to Section 2 and six-coordinate polymeric Mn(II) complex (**2**) was obtained from the reaction of $MnCl_2{\cdot}4H_2O$ with two molar equivalents of **1** in methanol.

The infrared spectrum of **1** shows characteristic phosphoryl and carbonyl stretches at 1193 and 1677 cm^{-1}, respectively. In the spectrum of the corresponding Mn(II) complex, a decrease for $\upsilon_{P=O}$ (1179 cm^{-1}) and slight increase for $\upsilon_{C=O}$ (1686 cm^{-1}) have been found in comparison to the free ligand. The observed negative shift of $\upsilon_{P=O}$ is in accord with coordination of the phosphoryl oxygen of the ligand to manganese [4, 7, 26], which was confirmed by X-ray crystallography. Increasing stretching wavenumber of pyridine ring upon complexation (1598 cm^{-1} in **1** and 1610 cm^{-1} in **2**) suggests that the ring nitrogen of the ligand also participates in coordination to Mn [35, 36]. Further, N–H stretching frequency increases on forming the complex, in agreement with the presence of weaker hydrogen bonds in complex in comparison to ligand [4]. The ν_{C-H} modes for aliphatic rings of **2** appear at 2923 and 2861 cm^{-1} and for aromatic ones at 3065 cm^{-1}. Weak bands at 483 and 428 cm^{-1} may be attributed to Mn–O and Mn–N vibrations.

The electronic spectrum of **1** in methanol shows a strong absorption at λ_{max} = 263 nm attributed to the π–π^* intraligand transition in pyridine [26]. By complexation, a blue shift has been observed in the value of the absorption (λ_{max} = 230 nm).

3.2. *Crystal structures*

Compound **1** crystallizes in the triclinic space group $P\bar{1}$ and **2** crystallizes in the hexagonal system with space group $R\bar{3}$ and $Z = 9$ in the unit cell. Molecular structures of **1** and **2** with the atom-labeling scheme are depicted in figures 1 and 2, respectively. Selected bond lengths and angles are summarized in tables S1 and S2 (see online supplemental material at http://dx.doi.org/10.1080/00958972.2013.863879).

The X-ray study of **2** reveals that **1** adopts a bidentate bridging mode and N_{py} and $O_{phosphoryl}$ are the preferred donors to Mn(II). Two *N*-coordinated and two *O*-coordinated ligands constitute the basal plane and two chlorides occupy the axial positions to form an octahedral geometry around Mn(II). The molecule is centrosymmetric and manganese occupies the center of inversion, so, the *trans* angles around manganese are exactly 180°. The cisoid O–Mn–N, N–Mn–Cl, and O–Mn–Cl angles deviate slightly from 90°, 86.80(5)–93.20(5)°, which indicates a slight distortion of the octahedral geometry.

The Mn–N distance (2.3083(15) Å) agrees with those found in other octahedral Mn(II) complexes with ligands containing pyridine [37, 38]. The Mn–O bond (2.1713(12) Å) is slightly longer than the reported values for Mn–$O_{phosphoryl}$ (2.115(2), 2.147(2) Å) in Mn$(Cl_3CC(O)NP(O)(NHC_3H_5)_2)_2$·Dipy [21], but is in the range of reported Mn(II) complexes with dichalcogenoimidodiphosphonate ligands [22–25].

The bond distances in the ligand change insignificantly from the free ligand to the complex. For instance, the P–N_{amine} bonds change from 1.6278(17) and 1.6374(18) Å in **1** to 1.623(2) and 1.6311(18) Å in **2**. No significant increase is observed for the P=O distance by complexation of the ligand (1.4819(14) Å in **1** *vs.* 1.4830(13) Å in **2**). Based on these observations, coordination to Mn(II) cation had no significant effect on the structure of the ligand.

Ligand **1** contains three potential donors (P=O, C=O and N_{py}) for coordination. CAPh can bind to a metal from both P=O and C=O groups as a chelate. However, coordination through phosphoryl is more probable as shown in our previous work [7]. Repulsion between carbonyl and phosphoryl dipoles in *O,O′*–donors, along with more polarizability of the P=O bond upon complexation, favors binding through phosphoryl [39]. On the other hand, we have previously shown that in the coordination of phosphorylated isonicotinamide and nicotinamide compounds to Sn [26], there is competition between phosphoryl and nitrogen of pyridine and binding occurs from either $O_{phosphoryl}$ or N_{py}. The ambidentate coordination pattern via both $O_{phosphoryl}$ and N_{py} producing 1-D chain has also been observed in complexation with Er [27]. Here, the same bonding pattern for **1** connects the

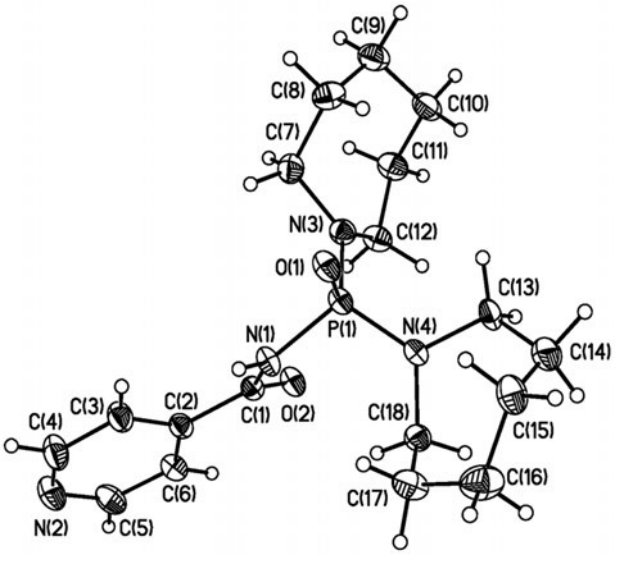

Figure 1. ORTEP drawing of **1** with numbering (50% probability ellipsoids).

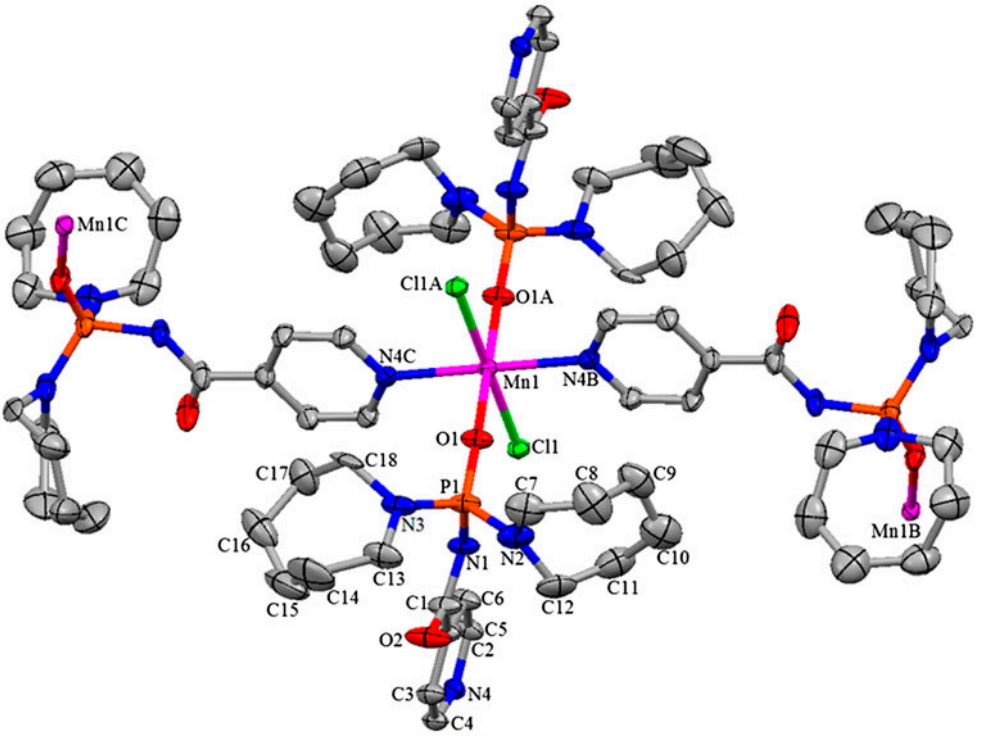

Figure 2. Molecular structure of **2** showing the atom numbering at 50% probability ellipsoids; hydrogens were omitted for clarity. Only major parts of disordered fragments are shown. Atoms denoted with A are generated by $-x$, $1-y$, $1-z$ symmetry code; those denoted with letters B and C are generated by $0.33-y$, $0.67+x-y$, $-0.33+z$ and $-0.33+y$, $0.33-x+y$, $1.33-z$ symmetry codes.

Mn(II) centers to afford a non-porous, 3-D polymeric network (figure 3). The 3-D network in our complex has been created by coordinative bonds rather than hydrogen bonding and π–π stacking interactions, which form 3-D supramolecular structures in reported Mn(II) complexes with *N,O*–donor ligands [40–42]. The only weak intramolecular hydrogen bonds appear between chloride and amidic protons. Hydrogen bond data are given in table 2. The Mn···Mn separation in the neighboring molecules is 9.665 Å.

Compound **1** produces centrosymmetric dimers via two equal intermolecular N(1)–H (1 N)···O(1)–P(1) hydrogen bonds. Oxygens of phosphoryl groups are also involved in weaker C(3)–H(3A)···O(1) intermolecular interactions with hydrogen of pyridine. Face-to-face π–π stacking interactions between the aromatic rings of adjacent dimers with centroid–centroid distance of 3.634 Å lead to the formation of 1-D chains in crystalline lattice (figure S1, Supplementary material).

In **1**, some of the carbons of one of the seven-membered amine rings (C(14), C(15), and C(14)) are disordered over two positions with an occupation ratio of 0.55 : 0.45. Also, in **2** C8–C12 and C14–C18 of seven-membered cycles are disordered over two positions with probabilities 0.80 : 0.20 and 0.6 : 0.4, respectively.

The phosphorus has a distorted tetrahedral configuration with bond angles of 105.72(9)–117.60(9)° and 104.24(7)–118.11(9)° in **1** and **2**, respectively. The phosphoryl and carbonyl groups are anti to each other as a result of dipole–dipole repulsion with 165.77(17)° and

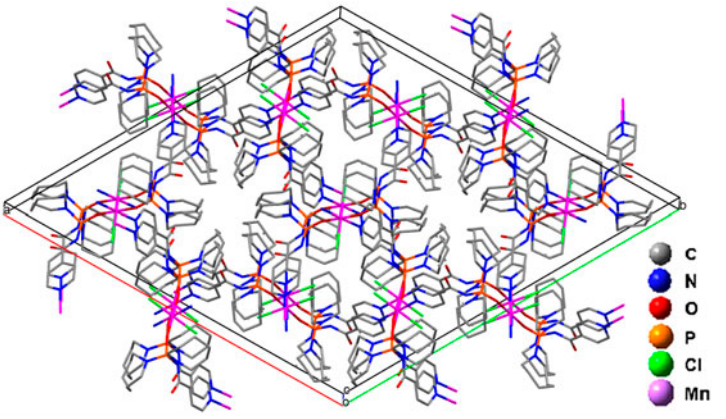

Figure 3. Crystal packing fragment of **2** showing the 3-D polymeric network.

Table 2. Hydrogen bond data for **1** and **2** (distances in Å and angles in °).

Compound	D–H···A	*d*(D–H)	*d*(H···A)	*d*(D···A)	∠DHA
1	N(1)–H(1N)···O(1) [$-x+1, -y+2, -z$]	0.81(3)	1.99(3)	2.802(3)	171(3)
	C(3)–H(3A)···O(1)	0.95(3)	2.335(1)	3.148(3)	143.2(1)
2	N(1)–H(1)···Cl(1) [x, y, z]	0.90	2.45	3.305(2)	159

−169.20(18)° for O–P–N–$C_{carbonyl}$ torsion angle in **1** and **2**, respectively. The P–N_{amide} bond length (1.6933(17) Å **1**, 1.6917(16) Å **2**) is longer than the P–N_{amine} distances (1.6278 (17)) and 1.6374(18) Å **1**, 1.623(2), and 1.6311(18) Å **2**) because of the resonance interaction of N_{amide} with the carbonyl π system [43, 44]. This interaction leads to partial multiple bond character in the C–N_{amide} bond (1.362(3) Å **1**, 1.367(2) Å **2**) and makes it shorter than C–N_{amine} distances (1.474(3)–1.479(2) Å **1**, 1.461(4)–1.509(6) Å **2**). All P–N bonds are shorter than the typical P–N single bond length (1.77 Å) [45], due to the electrostatic effects (polar bonds) which overlap with P–N σ bond [46].

3.3. *Characterization of nano-sized particles of 2*

We synthesized nano-sized particles of **2** by the addition of reagents in hexane-2-propanol under ultrasonic irradiation with the power of 138 W. Sonochemical treatment yields nanocrystalline particles due to the effect of acoustic cavitation. This process involves the formation, growth, and implosive collapse of microbubbles in liquid media, associated with the generation of local hot spots with ~5000 K temperature and about 1000 atm pressure, and cooling rates above 10^{10} K/s. These conditions enhance nucleation and crystallization [47].

Stretching frequencies observed in the IR spectra of single crystals of **2** and its nano-sized particles are identical. Figure S2a (Supplementary material) indicates a simulated XRD pattern based on the single crystal X-ray data and figures S2b and S2c (Supplementary material) show the experimental XRD patterns for the bulk and nano-sized powder of **2**, respectively. Simulated and experimental patterns are adequately matched with slightly different 2θ values, showing that the bulk material and nano-sized particles obtained by the

sonochemical process are the same with no indication of impurity phases. The small broadening of the XRD peaks of the nano-sized particles corresponds to a decrease in the particle size. The average crystallite size of nanocoordination polymer was calculated to be ~45 nm using the Debye–Scherrer equation [48]:

$$D = \frac{0.9\lambda}{\beta \cos\theta}$$

where D is the crystallite size, λ is the wavelength of X-ray radiation (0.154056 nm for Cu–Kα), β is the full-width at half maximum of the most intense diffraction peak, and θ is the Bragg angle.

SEM images of **2** bulk and nano-sized powders in two different scale bars are shown in figure 4(a)–(c). TEM image of nano-sized powder (figure 4(d)) shows that the particles are interconnected to some extent and possess almost irregular shape with an estimated mean size of 52 nm.

3.4. *VSM study*

The magnetic properties of **2** (bulk and nano-sized particles) were characterized by a VSM at room temperature and the magnetization curves are shown in figure 5. The lack of hysteresis as well as saturation even at high magnetic fields is an indication of paramagnetic behavior, originating from the non-interacting magnetic moments of Mn^{2+} ions at room

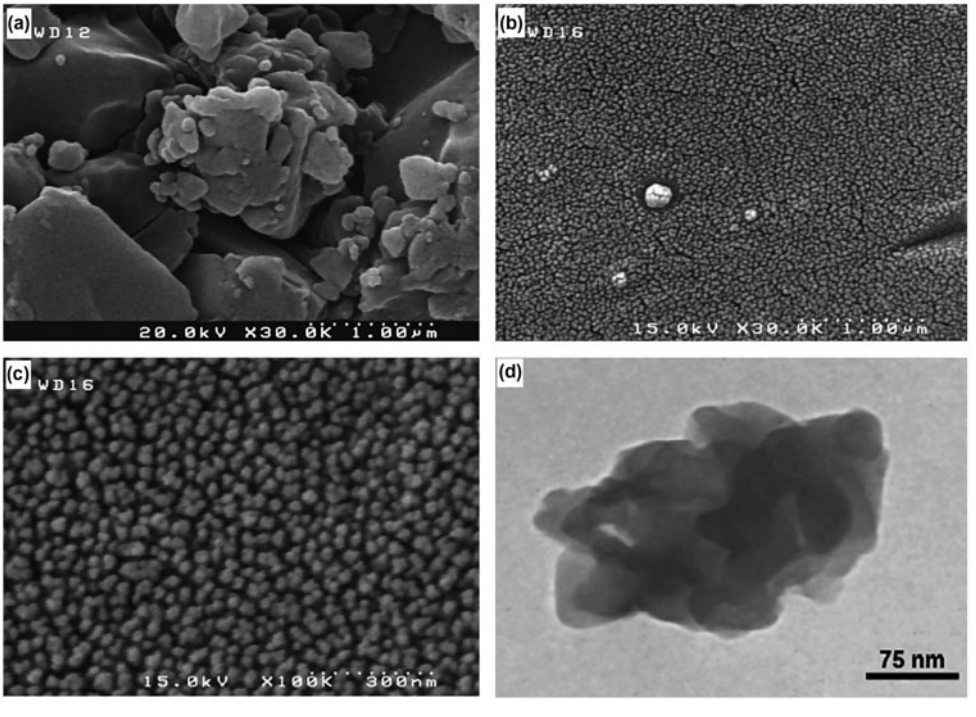

Figure 4. SEM images of **2** (a) bulk material; ((b), (c)) nanopolymer prepared by ultrasonic irradiation (in two different scale bars); (d) TEM image of nanopolymer **2**.

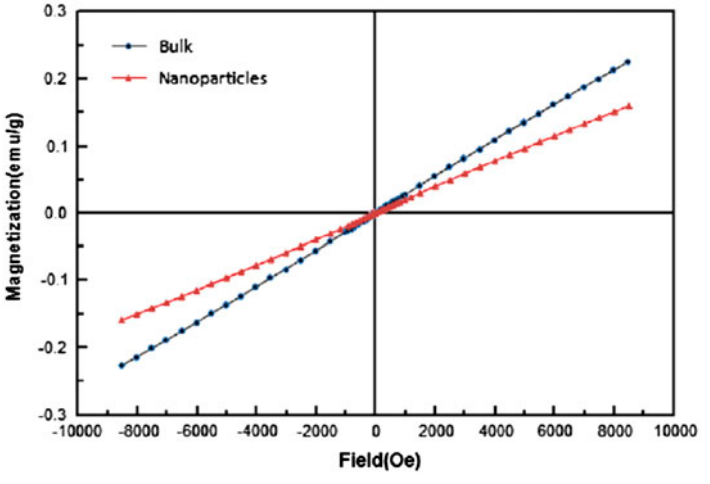

Figure 5. M–H curves of bulk powder and nano-sized particles of **2** at room temperature.

temperature. The value of magnetization for nano-sized particles of **2** at the highest applied field (0.16 emu/g in 85 kOe) is less than that of bulk powder (0.23 emu/g), which can be attributed to the small particle size effect. The energy of a magnetic particle in an external field is proportional to its volume via the number of magnetic molecules in a single magnetic domain. When this energy becomes comparable to kT, thermal fluctuations will reduce the total magnetic moment at a given field [49].

3.5. *Thermal study of 2 and characterization of products*

To study the thermal stability of **2**, TG and DTA were conducted in static air between 40 and 600 °C. The complex shows a two-stage decomposition (figure 6, black lines). The first step occurs at 181–300 °C and could be ascribed to the thermal removal of chlorides as well as amide groups with an estimated mass loss of 30% (Calcd 32.9%). This stage is associated with a broad exothermic DTA peak around 298 °C. Above 320 °C, the complex decomposes in a gradual manner which corresponds to thermal degradation of amine groups, with two accompanying exothermic DTA peaks at 445 and 460 °C Decomposition of nano-sized particles of **2** (figure 6, red lines) starts about 20 degrees earlier than its bulk counterpart with an estimated mass loss of 52% in the first step, showing less thermal stability compared to the single crystals. This is probably due to higher surface-to-volume ratio of the smaller particles, as destruction of the lattices in a single crystal needs more heat. The DTA curve of nano-sized material represents three exothermic peaks at 287, 452, and 492 °C in accord with those observed in the DTA curve of the bulk counterpart. The XRD pattern of the final residue obtained by calcination of compound **2** bulk powder and also its nano-sized particles at 600 °C in air are shown in figure S3 (Supplementary material). All detectable peaks are indexed as manganese pyrophosphate ($Mn_2P_2O_7$) and manganese cyclotetraphosphate ($Mn_2P_4O_{12}$) with their structures in standard data as JCPDS card numbers 29-0891 and 36-0210, respectively. These results indicate that $Mn_2P_2O_7$ crystal structure is in the monoclinic system with the lattice parameters a = 6.636 Å, b = 8.584 Å, c = 4.5457 Å, β = 102.78°, SG = *C2/m*, and Z = 2.

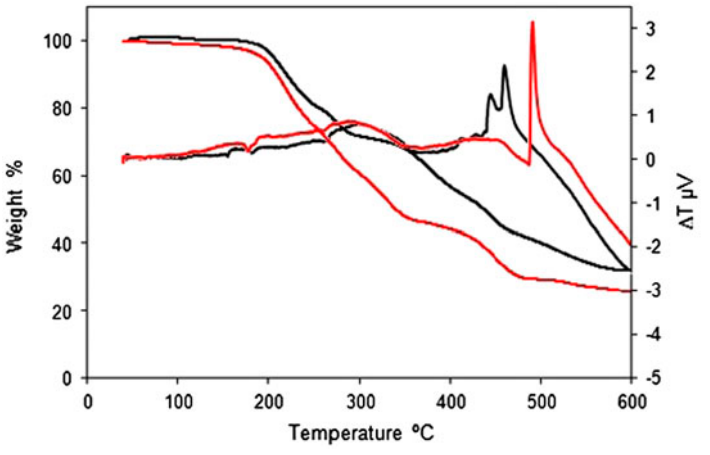

Figure 6. Thermal behavior of bulk (black lines) and nano-sized particles (red lines) of **2** (see http://dx.doi.org/10.1080/00958972.2013.863879 for color version).

Thermal decomposition of coordination polymers and metal complexes is a useful approach to obtain inorganic nano-sized materials with diverse morphologies [50]. The SEM images of the calcination products of bulk and nano-sized powders of **2** are shown in figure 7(a) and (b), respectively, indicating the formation of manganese phosphates in two

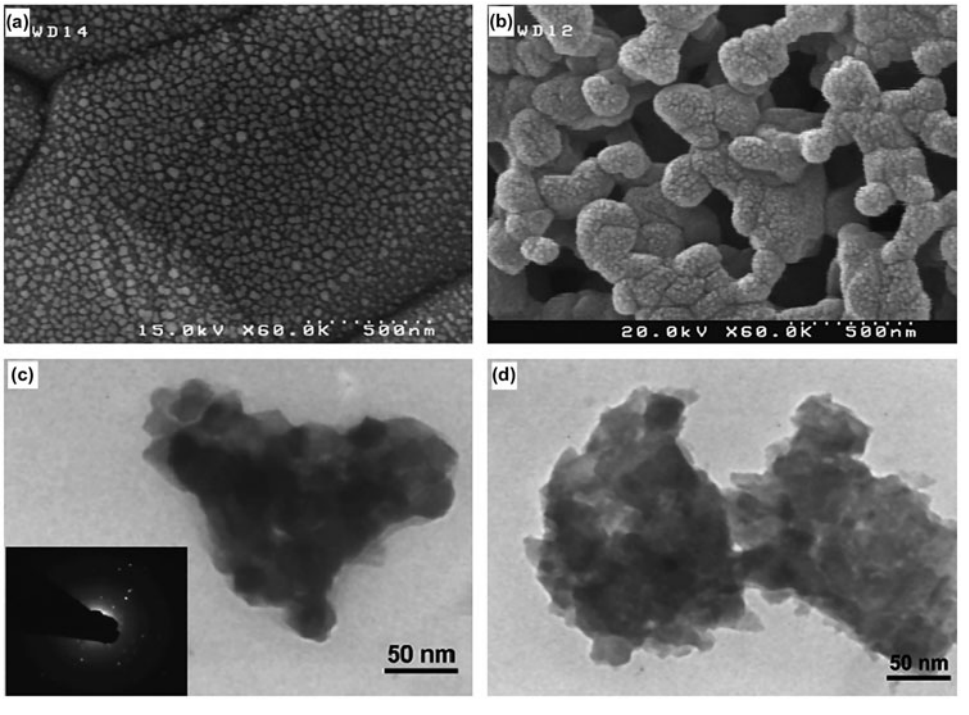

Figure 7. SEM images of manganese phosphate particles obtained by calcination of (a) bulk and (b) nanopolymer **2**, TEM images of calcination product of (c) (inset SAED pattern) bulk and (d) nanopolymer **2**.

different morphologies. TEM image (figure 7(c)) shows that the thermal residue of bulk powder of **2** is composed of square particles with some degree of aggregation (mean particle size of about 34 ± 10 nm). The rings and spots in the corresponding selected area electron diffraction (SAED) pattern (figure 7(c), inset) indicate the crystalline nature of the product. The TEM image of calcination product of nanopowder of **2** (figure 7(d)) shows the formation of submicron objects composed of densely aggregated particles (average diameter of 24 ± 7 nm). The morphology of the obtained manganese phosphates as well as the synthesis route are different from those reported [51, 52]. These experiments indicate that the particle size of the starting powder influences the morphology and size of the final decomposition products. Further, the morphology of manganese phosphates is quite different from the starting material.

4. Conclusions

A new *N*,*O*–donor phosphoramide and its Mn(II) complex were obtained. X-ray analysis revealed that **2** has a polymeric structure which extends in 3-D by coordinative bonds. Mn (II) is six coordinate with a slightly distorted octahedral geometry. Nano-sized particles of **2** were generated by sonochemical irradiation and powder XRD, and IR studies confirmed that the nano-sized and bulk materials are the same. Compound **2** has paramagnetic behavior at room temperature and less magnetization was observed for its nanoscale powder. A mixture of manganese phosphates was obtained by a thermal treatment of **2**.

Supplementary material

CCDC 742033 and 786391 contain the supplementary crystallographic data for **1** and **2**, respectively. These data can be obtained free of charge from The Cambridge Crystallographic Data Center via www.ccdc.cam.ac.uk/data_request/cif.

Acknowledgement

Financial support of this work by Tarbiat Modares University is gratefully acknowledged.

References

[1] J.-C. Bollinger, J. Levy-serpier, J. Debord, B. Penicaut. *J. Enzyme Inhib. Med. Chem.*, **3**, 211 (1990).
[2] K. Gholivand, Z. Shariatinia, K. Khajeh, H. Naderimanesh. *J. Enzyme Inhib. Med. Chem.*, **21**, 31 (2006).
[3] R.K. Andrews, A. Dexter, R.L. Blakeley, B. Zerner. *J. Am. Chem. Soc.*, **108**, 7124 (1986).
[4] K. Gholivand, H.R. Mahzouni, M. Pourayoubi, S. Amiri. *Inorg. Chim. Acta*, **363**, 2318 (2010).
[5] K.E. Gubina, V.A. Ovchynnikov, V.M. Amirkhanov, H. Fischer, R. Stumpf, V.V. Skopenko. *Z. Naturforsch*, **55b**, 576 (2000).
[6] K.E. Gubina, V.A. Ovchynnikov, J. Swiatek-Kozlowska, V.M. Amirkhanov, T.Y. Sliva, K.V. Domasevitch. *Polyhedron*, **21**, 963 (2002).
[7] K. Gholivand, S. Farshadian. *Inorg. Chim. Acta*, **368**, 111 (2011).
[8] K. Gholivand, Z. Shariatinia. *J. Organomet. Chem.*, **691**, 4215 (2006).
[9] K. Gholivand, H. Mostaanzadeh, T. Koval, M. Dusek, M.F. Erben, H. Stoeckli-Evans, C.O. Della Védova. *Acta Cryst.*, **B66**, 441 (2010).
[10] K. Gholivand, S. Farshadian, Z. Hosseini. *J. Organomet. Chem.*, **696**, 4298 (2012).
[11] E.A. Trush, V.M. Amirkhanov, V.A. Ovchynnikov, J. Swiatek-Kozlowska, K.A. Lanikina, K.V. Domasevitch. *Polyhedron*, **22**, 1221 (2003).
[12] Z. Guo, P.J. Sadler. *Angew. Chem. Int. Ed.*, **38**, 1512 (1999).

[13] V.L. Pecoraro. *Manganese Redox Enzymes*, VCH, New York (1992).
[14] O. Sengupta, P.S. Mukherjee. *Inorg. Chem.*, **49**, 8583 (2010).
[15] D. Pinkowicz, R. Pelka, O. Drath, W. Nitek, M. Balanda, A.M. Majcher, G. Poneti, B. Sieklucka. *Inorg. Chem.*, **49**, 7565 (2010).
[16] H.W. Kuay, T.A. Okamura, W.Y. Sun. *J. Coord. Chem.*, **65**, 3147 (2012).
[17] K. Gholivand, S. Farshadian, Z. Hosseini, K. Khajeh, N. Akbari. *Appl. Organomet. Chem.*, **24**, 700 (2010).
[18] V.A. Ovchynnikov, V.M. Amirkhanov, A.A. Kapshuk, T.Y. Sliva, T. Glowiak, H. Kozlowski. *Z. Naturforsch*, **53b**, 836 (1998).
[19] E.A. Trush, V.A. Ovchynnikov, K.V. Domasevitch, J. Swiatek-Kozlowska, V.Y. Zub, V.M. Amirkhanov. *Z. Naturforsch*, **57b**, 746 (2002).
[20] V.A. Trush, K.E. Gubina, V.M. Amirkhanov, J. Swiatek-Kozlowska, K.V. Domasevitch. *Polyhedron*, **24**, 1007 (2005).
[21] K.E. Gubina, O.A. Maslov, E.A. Trush, V.A. Trush, V.A. Ovchynnikov, S.V. Shishkina, V.M. Amirkhanov. *Polyhedron*, **28**, 2661 (2009).
[22] I. Szekely, C. Silvestru, J.E. Drake, G. Balazs, S.I. Farcas, I. Haiduc. *Inorg. Chim. Acta*, **299**, 247 (2000).
[23] I. Szekely, J.E. Drake, C. Silvestru. *Phosphorus, Sulfur Silicon*, **124–125**, 557 (1997).
[24] A.M. Preda, A. Silvestru, S. Farcas, A. Bienko, J. Mrozinski, M. Andruh. *Polyhedron*, **27**, 2905 (2008).
[25] W. Shi, L. Zhang, M. Shafaei-Fallah, A. Rothenberger. *Z. Anorg. Allg. Chem.*, **633**, 440 (2007).
[26] K. Gholivand, N. Oroujzadeh, F. Afshar. *J. Organomet. Chem.*, **695**, 1383 (2010).
[27] K. Gholivand, N. Oroujzadeh, M. Rajabi. *J. Iran. Chem. Soc.*, **9**, 865 (2012).
[28] M. Yamada, M. Arai, M. Kurihara, M. Sakamoto, M. Miyake. *J. Am. Chem. Soc.*, **126**, 9482 (2004).
[29] Bruker, *SAINTPLUS*, v. 6.01, *Data Reduction and Correction Program*, Bruker AXS, Madison, WI, USA (1998).
[30] Bruker, *SMART*, v. 5.059, *Bruker Molecular Analysis Research Tool*, Bruker AXS, Madison, WI, USA (1998).
[31] Bruker APEX2 Software Package, Bruker AXS Inc., 5465 East Cheryl Parkway, Madison, WI 53711, USA (2005).
[32] G.M. Sheldrick, *SADABS*, v. 2.01, *Bruker/Siemens Area Detector Absorption Correction Program*, Bruker AXS, Madison, WI, USA (1998).
[33] G.M. Sheldrick, *SHELXTL*, v. 5.10, *Structure Determination Software Suite*, Bruker AXS, Madison, WI, USA (1998).
[34] K. Gholivand, F. Afshar, Z. Shariatinia, K. Zare. *Struct. Chem.*, **21**, 629 (2010).
[35] S. Yurdakul, A. Atac, E. Sahin, S. Ide. *Vib. Spectrosc.*, **31**, 41 (2003).
[36] A. Atac, S. Yurdakul, S. Ide. *J. Mol. Struct.*, **783**, 79 (2006).
[37] W. Park, J.H. Cho, H.I. Lee, M. Park, M.S. Lah, D. Lim. *Polyhedron*, **27**, 2043 (2008).
[38] X. Zhang, K. Cheng. *J. Coord. Chem.*, **65**, 3019 (2012).
[39] C. Boehme, G. Wipff. *Inorg. Chem.*, **41**, 727 (2002).
[40] X. Feng, Y.Y. Wang, Y.C. Hu, S.P. Chen, W.J. Zhao, X.W. Yang. *J. Coord. Chem.*, **65**, 2692 (2012).
[41] J.P. Zou, S.C. Dai, W.T. Guan, H.B. Yang, Y.F. Feng, X.B. Luo. *J. Coord. Chem.*, **65**, 2877 (2012).
[42] T.T. Cao, Y. Ma, C. Yang, D.Z. Liao, S.P. Yan. *J. Coord. Chem.*, **63**, 3093 (2010).
[43] A.G. Iriarte, M.F. Erben, K. Gholivand, J.L. Jios, S.E. Ulic, C.O. Della. Vedova, *J. Mol. Struct.*, **886**, 66 (2008).
[44] A.G. Iriarte, E.H. Cutin, M.F. Erben, S.E. Ulic, J.L. Jios, C.O. Della Vedova. *Vib. Spectrosc.*, **46**, 107 (2008).
[45] D.E.C. Corbridge. *Phosphorus: An Outline of its Chemistry, Biochemistry and Technology*, 5th Edn, Elsevier, Amsterdam (1995).
[46] D.G. Gilheany. *Chem. Rev.*, **94**, 1339 (1994).
[47] (a) K.S. Suslick, G.J. Price. *Annu. Rev. Mater. Sci.*, **29**, 295 (1999); (b) D.K. Buĉar, L.R. MacGillivray. *J. Am. Chem. Soc.*, **129**, 32 (2007).
[48] B.D. Cullity, *Elements of X-ray Diffraction*, 2nd Edn, Addison-Wesley, Reading (1978).
[49] K.V.P.M. Shafi, A. Gedanken. *Chem. Mater.*, **10**, 3445 (1998).
[50] (a) C.R. Bhattacharjee, D.D. Purkayastha, J.R. Chetia. *J. Coord. Chem.*, **64**, 4434 (2011); (b) R. Gupta, S. Sanotra, H.N. Sheikh, B.L. Kalsotra, V.K. Gupta Rajnikant. *J. Coord. Chem.*, **65**, 3917 (2012).
[51] S. Wang, X. Jiang, G. Du, Z. Guo, J. Jang, S.J. Kim. *Mater. Lett.*, **65**, 3265 (2011).
[52] (a) C. Danvirutai, B. Boonchom, S. Youngmea. *J. Alloys Compd.*, **457**, 75 (2008); (b) B. Boonchom, R. Baitahe. *Mater. Lett.*, **63**, 2218 (2009).